THREE-DIMENSIONAL SPLINE-GENERATED COORDINATE TRANSFORMATIONS FOR GRIDS AROUND WING-BODY CONFIGURATIONS

Lars-Erik Eriksson
The Aeronautical Research Institute of Sweden (FFA)

ABSTRACT

In this work, a direct algebraic method has been developed and applied to generate three-dimensional grids around wing-body configurations. The method used is a generalized transfinite interpolation method which generates the desired coordinate transformation using geometric data only on the boundaries of the domain of interest. The geometric data that can be specified includes not only coordinates on the boundaries but also out-of-surface parametric derivatives that give a very precise control over the transformation in the vicinity of the surface. In addition to this, the method gives good control over the stretching of the mesh between different boundaries.

The topology of the transformation chosen for the wing-body problem is of a novel type which gives a grid that wraps around not only the leading edge of the wing, but also the wing tip. The body is represented by a deformation of the plane-of-symmetry.

For mesh verification, a simple finite element type algorithm is used to solve the Laplace equation (incompressible flow) on the mesh in question. By varying the details of the matrix evaluation process it is possible to obtain solutions which are more or less dependent on the global mesh properties and thereby get a measure of the "quality" of the mesh. This is essential for applications where for example finite volume methods are used, since these methods depend on smooth global properties of the mesh.

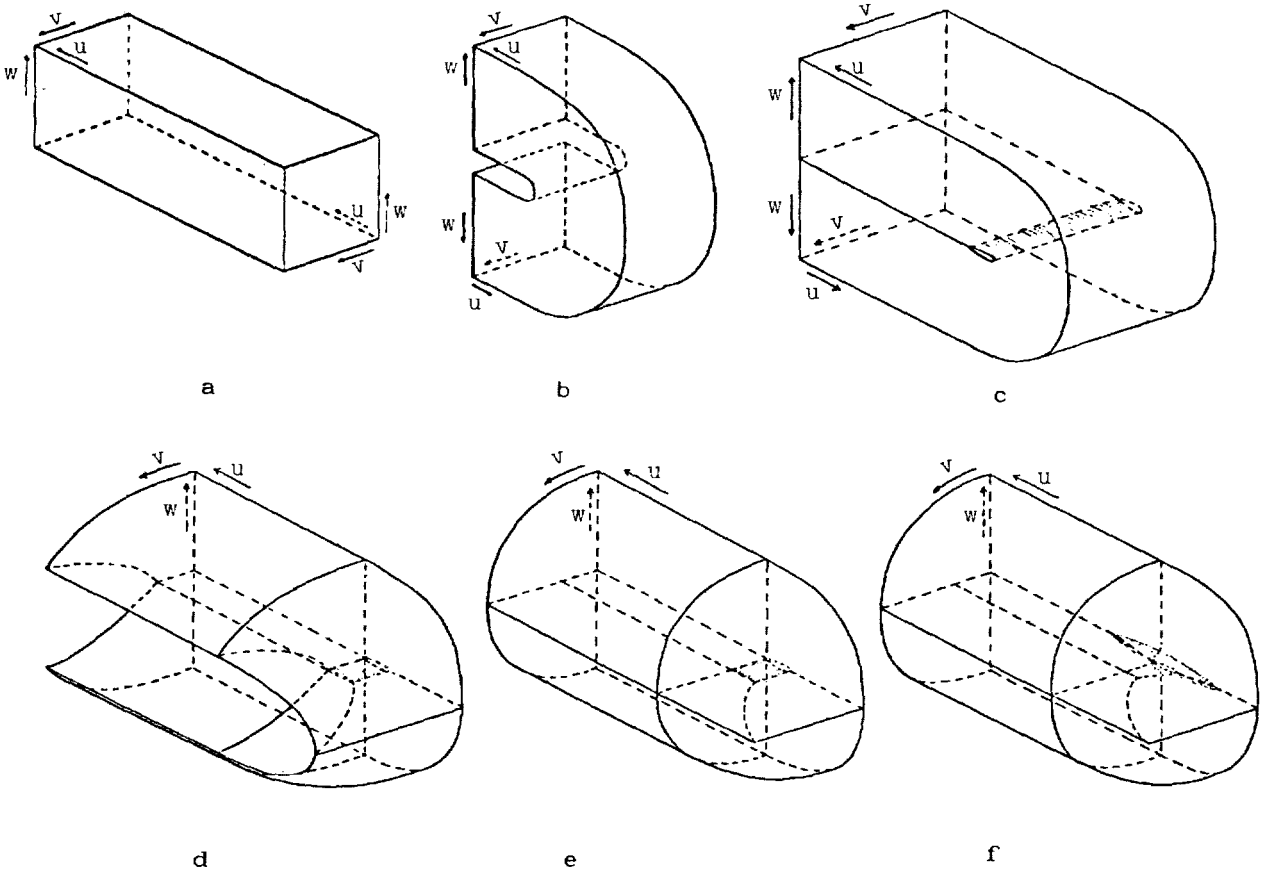

Fig. 1. Topology of wing-body transformation.

The topology of the transformation used for the wing-body problem is outlined by these schematic figures. In the top left figure, the computational or parametric domain is shown with u,v,w as arbitrary parameters. The top middle and right figures illustrate the first step in the transformation, which is a "folding" process to obtain a wing-like inner boundary and an internal branch cut behind the wing trailing edge. The next step is shown in the bottom left and middle figures and consists of another "folding" process in the spanwise direction of the wing. This results in the collapse of a surface into another internal branch cut outside the wing and wake. The last figure shows the third and last step, introducing the body. This is done by deforming the plane-of-symmetry boundary and displacing the wing and wake appropriately.

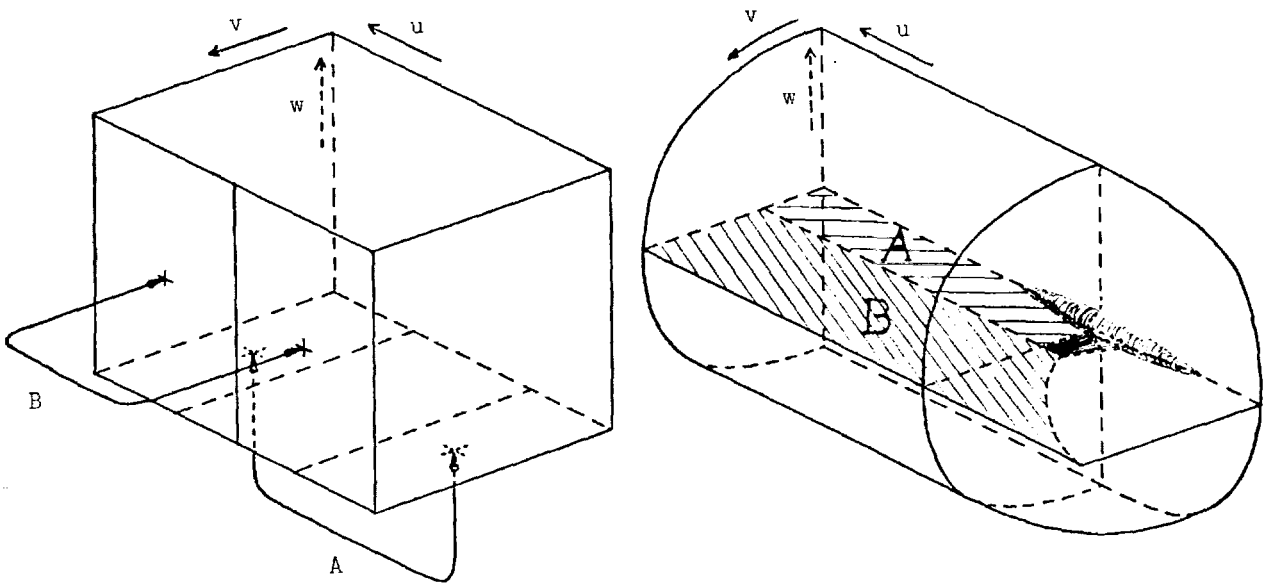

Fig. 2. Internal branch cuts.

The internal branch cuts are shown in both the parametric domain and the physical domain. For actual flow computations in the parametric domain, the usual boundary conditions have to be supplemented by appropriate continuity conditions at the branch cuts.

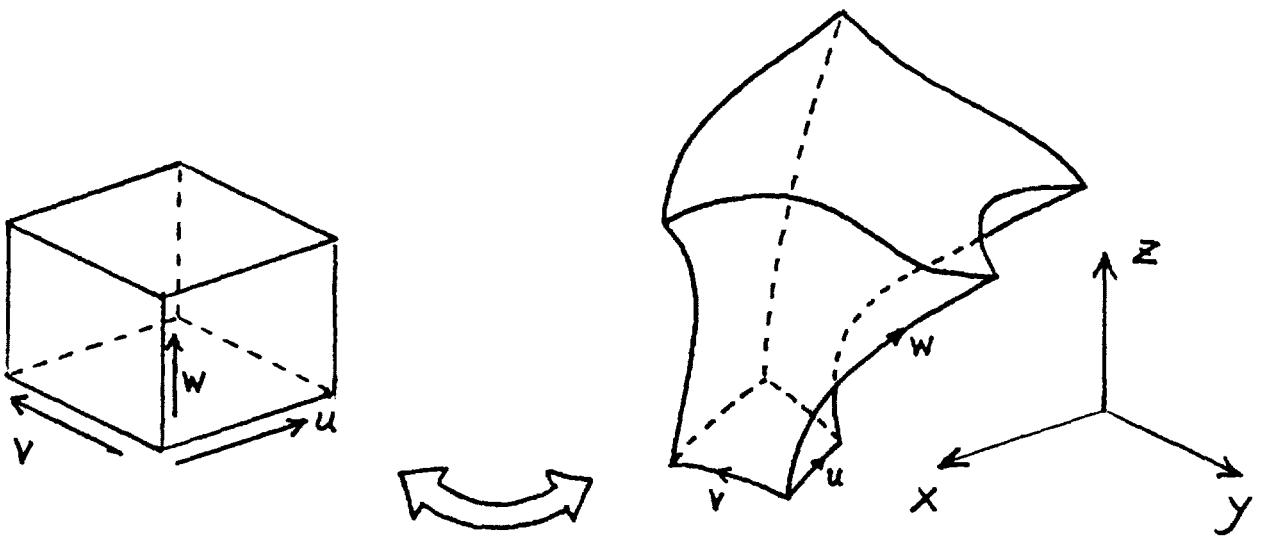

$$\begin{cases} x = x(u,v,w) \\ y = y(u,v,w) \\ z = z(u,v,w) \end{cases}$$

Fig. 3. Transfinite Interpolation

To generate the desired transformation, a generalized transfinite interpolation method is used. This procedure (which alternately can be viewed as a generalized spline interpolation procedure) gives a transformation by interpolating geometric data from the six boundaries of the parametric domain into the interior of this domain. The geometric data needed for this method consists of coordinates and out-of-surface parametric derivatives. With appropriate choices of coordinates and derivatives it is also possible to generate some boundaries automatically, thus reducing the number of boundaries that have to be specified.

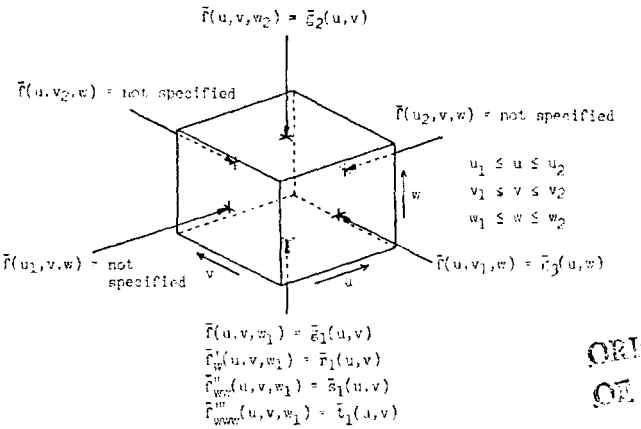

Fig. 4. Application of the transfinite interpolation method to the wing-body transformation.

This figure shows the parametric domain and the geometric data needed to generate the wing-body transformation. The vector valued function $\bar{f}(u,v,w)$ is here the desired transformation $[x(u,v,w),y(u,v,w),z(u,v,w)]$ and is specified only on three of the six boundaries: the plane $w=w_1$ (=the transformed wing and wake surface), the plane $w=w_2$ (=the transformed outer boundary) and the plane $v=v_1$ (=the transformed body and plane-of-symmetry boundary). On the plane $w=w_1$, there are also out-of-surface parametric derivatives $\bar{f}'_w$, $\bar{f}''_{ww}$, $\bar{f}'''_{www}$ specified. These parametric derivatives are essential to give a precise control over the transformation near the wing surface and are also necessary to generate automatically the geometric data for the remaining three boundaries. The choice of first, second and third derivatives is arbitrary (it is possible to specify any number of derivatives), but has been found to give good results.

To generate the transformation $\bar{f}(u,v,w)$ it is necessary to introduce blending functions $\beta_1(v)$; $v_1 \le v \le v_2$ and $\gamma_1(w)$, $\gamma_2(w)$, $\gamma_3(w)$, $\gamma_4(w)$, $\gamma_5(w)$; $w_1 \le w \le w_2$ with conditions:

$\beta_1(v_1) = 1$	$\gamma_1(w_1) = 1$	$\gamma_2(w_1) = 0$	$\gamma_3(w_1) = 0$	$\gamma_4(w_1) = 0$	$\gamma_5(w_1) = 0$
$\beta_1(v_2) = 0$	$\gamma_1'(w_1) = 0$	$\gamma_2'(w_1) = 1$	$\gamma_3'(w_1) = 0$	$\gamma_4'(w_1) = 0$	$\gamma_5'(w_1) = 0$
	$\gamma_1''(w_1) = 0$	$\gamma_2''(w_1) = 0$	$\gamma_3''(w_1) = 1$	$\gamma_4''(w_1) = 0$	$\gamma_5''(w_1) = 0$
	$\gamma_1'''(w_1) = 0$	$\gamma_2'''(w_1) = 0$	$\gamma_3'''(w_1) = 0$	$\gamma_4'''(w_1) = 1$	$\gamma_5'''(w_1) = 0$
	$\gamma_1(w_2) = 0$	$\gamma_2(w_2) = 0$	$\gamma_3(w_2) = 0$	$\gamma_4(w_2) = 0$	$\gamma_5(w_2) = 1$

The transfinite interpolation scheme is then defined by

1. $\bar{f}^*(u,v,w) = \gamma_1(w)\bar{g}_1(u,v) + \gamma_2(w)\bar{r}_1(u,v) + \gamma_3(w)\bar{s}_1(u,v) + \gamma_4(w)\bar{t}_1(u,v) + \gamma_5(w)\bar{g}_2(u,v)$

2. $\bar{f}(u,v,w) = \bar{f}^*(u,v,w) + \beta_1(v)[\bar{g}_3(u,w) - \bar{f}^*(u,v_1,w)]$

The choice of blending functions has to be made with care, since they have a direct influence on the "stretching" of the transformation between different boundaries.

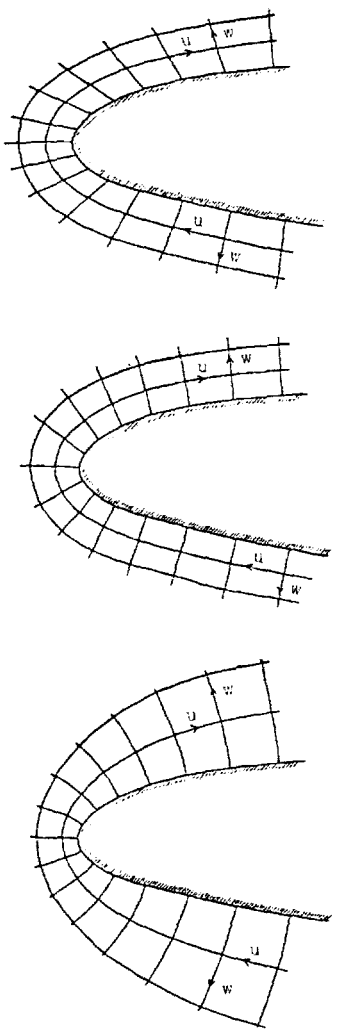

Fig. 5. Effect of out-of-surface parametric derivatives.

These three figures show the importance of the out-of-surface parametric derivatives that must be specified on the wing and wake boundary. The top figure illustrates the case where only the first derivative $[x'_w, y'_w, z'_w]$ is specified. This derivative determines the direction of the outgoing grid lines (lines with constant u and v) and the spacing between successive grid surfaces (surfaces with constant w). To obtain a univalent transformation, the derivative must be adapted to the surface geometry and also vary smoothly. An obvious way to adapt the derivative is to make it orthogonal to the surface (middle figure). If the radius of curvature varies very rapidly however, this simple solution does not work very well, because it requires an excessive concentration of grid points in the critical region. A better solution is to specify higher derivatives, for example $[x''_{ww}, y''_{ww}, z''_{ww}]$ and $[x'''_{www}, y'''_{www}, z'''_{www}]$. With these derivatives, it is possible to obtain a great variety of transformations near the wing surface. The bottom figure shows an example where the transformation is approximately conformal in the vicinity of the wing.

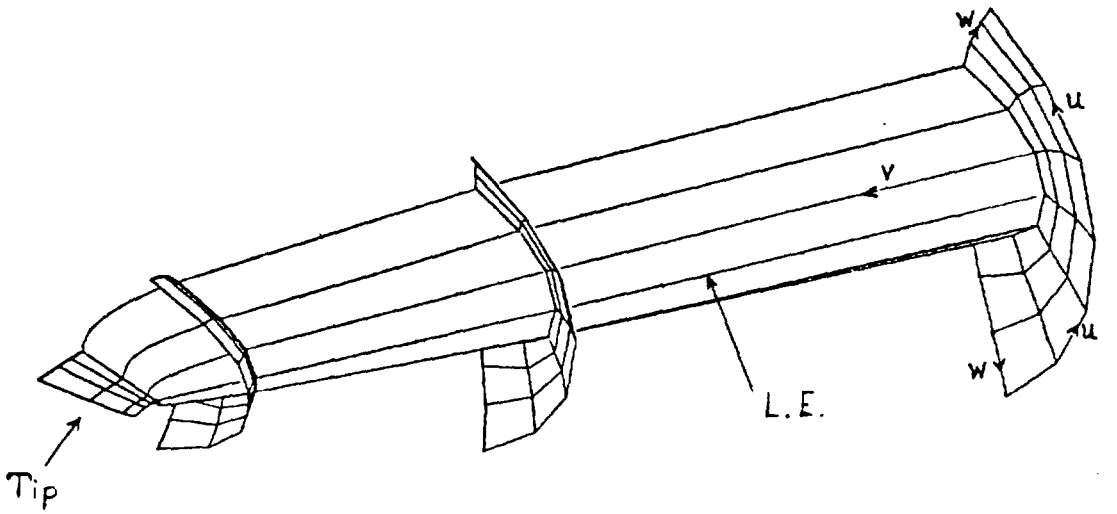

Fig. 6. Detail of typical grid in the leading edge/tip region.

In order to obtain the desired behaviour of the transformation in the leading edge/tip region of the wing, it is necessary to specify the out-of-surface parametric derivatives as smooth functions of both the in-surface parameters u and v. This figure is an oblique view of a typical grid in this region and shows how the constant-v surfaces gradually collapse into the branch cut outside the wing tip as the v-parameter is increased towards the maximum value.

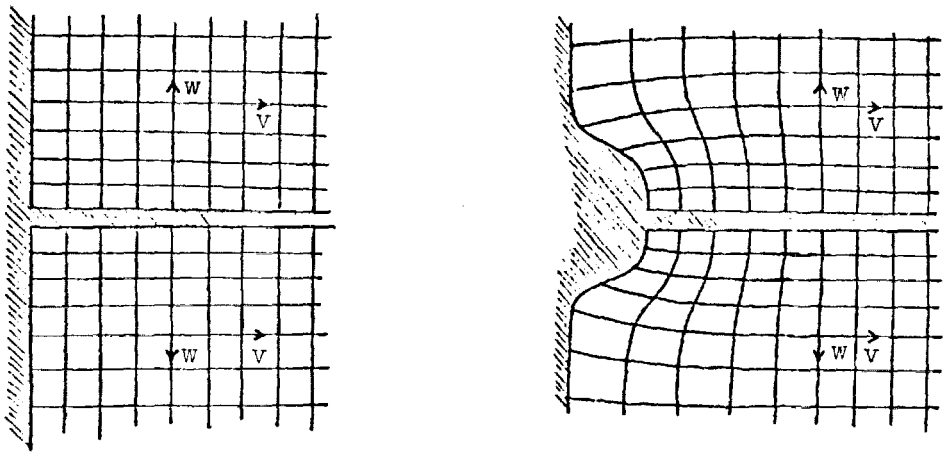

Fig. 7. Deforming the plane-of-symmetry to represent the body.

This figure shows the effect on the transformation of deforming the plane-of-symmetry to simulate a half-body. The wing and wake surface is translated outwards and the deformation is interpolated into the domain in a smooth manner that is determined by the blending function $\beta_1(v)$. Since the deformed plane-of-symmetry is specified in terms of coordinates, it is also possible to concentrate the grid lines around the body as shown by the figure.

Shown in figure 8 are several views of a wing-body grid. Figures 8(a) and 8(b) show from two perspective views:

- the upper half of the wing and wake surface
- the upper half of the deformed plane-of-symmetry
- the internal branch cut outside the wing and wake
- one of the downstream boundaries
- the constant-u surface that emanates from the wing leading edge

Figures 8(c) and 8(d) show a constant-v surface of the same grid as in figure 8(a). This surface emanates approximately from the mid section of the wing.

Figures 8(e) and 8(f) show two constant-u surfaces of the same grid as in figure 8(a). These surfaces emanate from the upper and lower x/c = 0.25 lines.

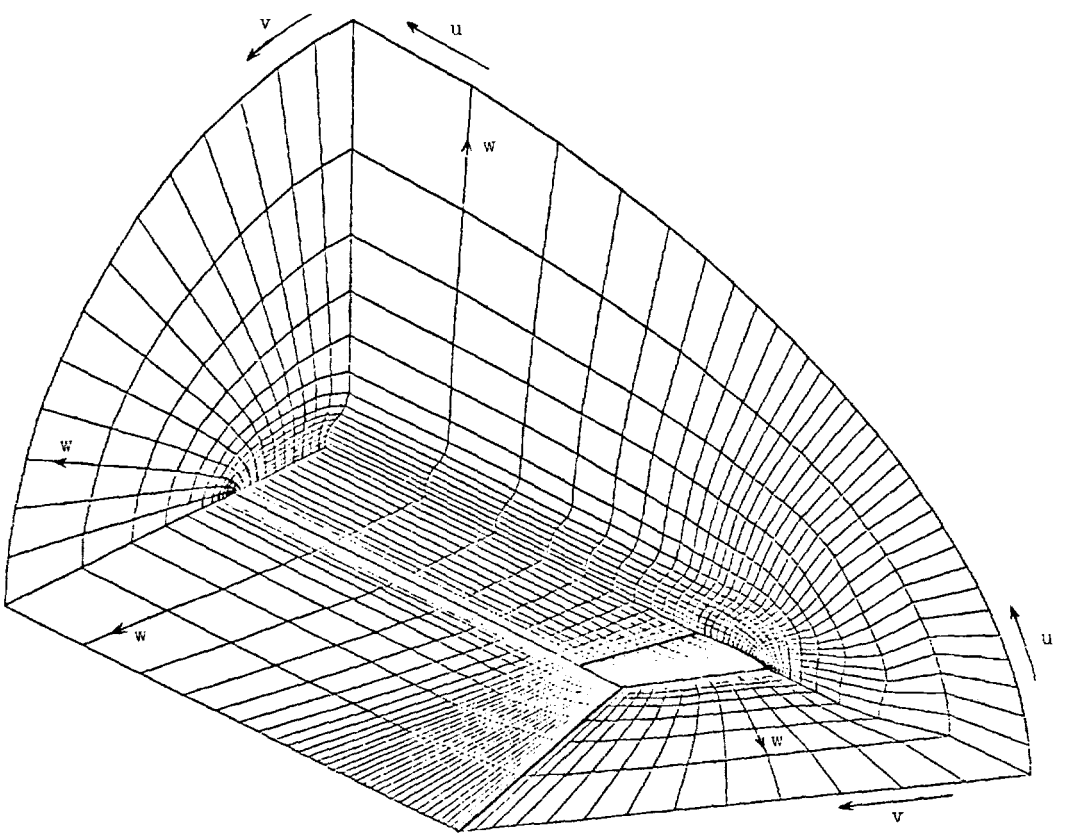

(a) Wing-body grid viewed from below.

Figure 8.- Wing-body grid.

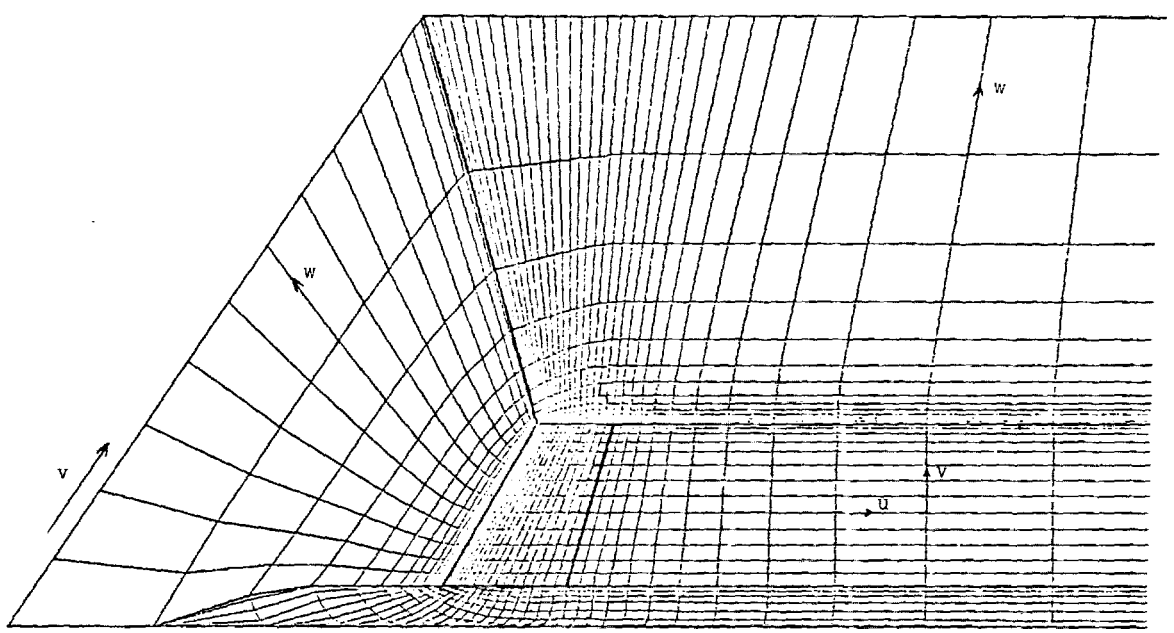

(b) Wing-body grid viewed from above.

Figure 8.- Continued.

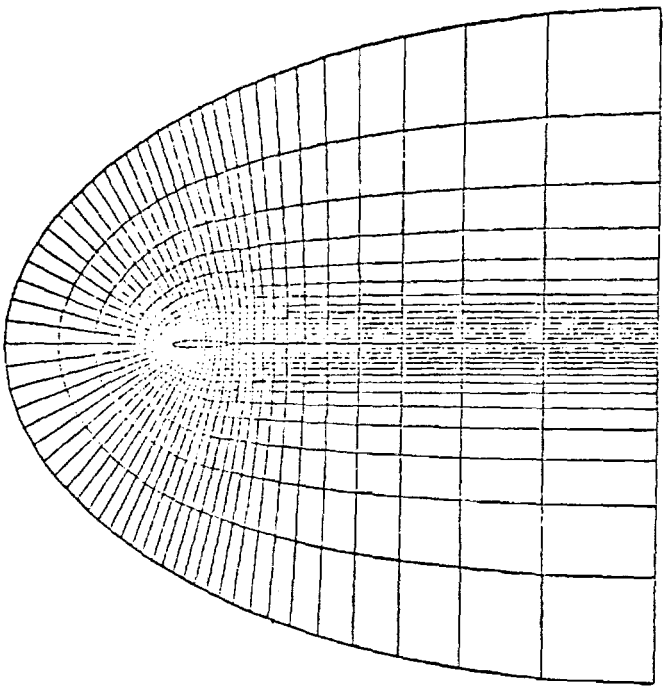

(c) Planar view of wing-body grid in wing wake region.

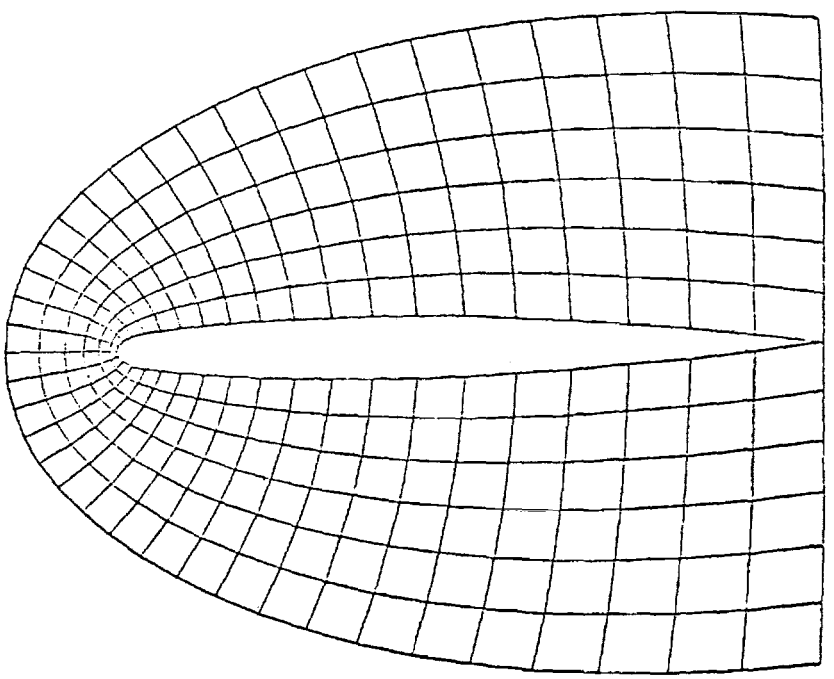

(d) Enlarged view of grid at wing surface.

Figure 8.- Continued.

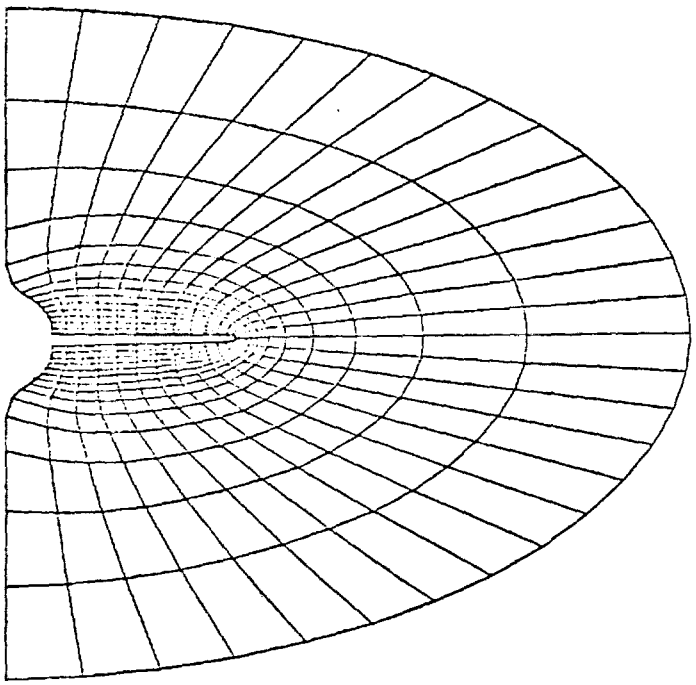

(e) Planar view of wing-body grid perpendicular to the body axis.

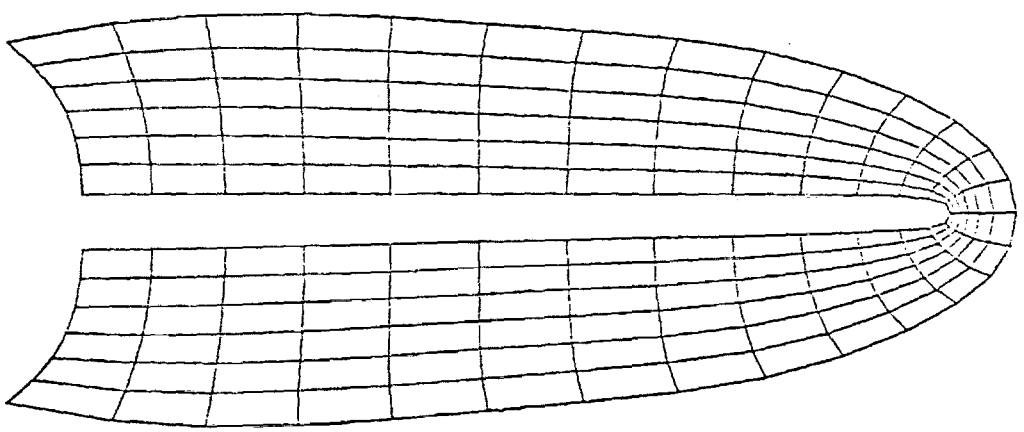

(f) Enlargement of planar view.

Figure 8.- Concluded.